

Energy Conversion within Current Sheets in the Earth's Quasi-parallel Magnetosheath

Steven J Schwartz^{1*†}, Harald Kucharek², Charles J Farrugia², K.J. Trattner¹,
Imogen Gingell³, Robert Ergun¹, Robert Strangeway⁴, Daniel Gershman⁵

¹Laboratory for Atmospheric and Space Physics, CU Boulder, Boulder, CO

²University of New Hampshire, Durham, NH

³Physics and Astronomy, University of Southampton, Southampton, UK

⁴UCLA, Los Angeles, CA

⁵Goddard Space Flight Center, Greenbelt, MD

Key Points:

- Intense current events are distributed uniformly downstream of a quasi-parallel bow shock.
- The events are associated primarily with a conversion of field energy into particle energy.
- The energy processed by these events is a non-negligible fraction of the energy incident at the bow shock.

Manuscript Date 11/24/2020

*Laboratory for Atmospheric and Space Physics, CU Boulder, Boulder, CO

†Also Emeritus Professor, Imperial College London

Corresponding author: Steven Schwartz, steven.schwartz@lasp.colorado.edu

Abstract

Shock waves in collisionless plasmas rely on kinetic processes to convert the primary incident bulk flow energy into thermal energy. That conversion is initiated within a thin transition layer but may continue well into the downstream region. At the Earth's bow shock, the region downstream of shock locations where the interplanetary magnetic field is nearly parallel to the shock normal is highly turbulent. We study the distribution of thin current events in this magnetosheath. Quantification of the energy dissipation rate made by the MMS spacecraft shows that these isolated intense currents are distributed uniformly throughout the magnetosheath and convert a significant fraction (5%-11%) of the energy flux incident at the bow shock.

Plain Language Summary

Shock waves form when a supersonic flow encounters an immovable object. Thus, ahead of the magnetic bubble formed by the Earth's extended magnetic field, the flow of charged particles emanating from the Sun known as the solar wind is shocked, slowed, and deflected around the Earth. In dense fluids, the conversion of the incident bulk flow energy into heat is accomplished by collisions between particles or molecules. However, the solar wind is so rarefied that such collisions are negligible, and the energy conversion involves more than one kinetic process that couples the different particles to the electromagnetic fields. Under some orientations of the interplanetary magnetic field carried by the wind, the shocked medium is highly turbulent. Within that turbulence are isolated thin regions carrying large electric currents. We have studied those currents, and find that they are converting energy from one form to another at a rate that is a significant fraction of the incident energy flux. Thus, these currents contribute significantly to the overall shock energetics.

1 Introduction

Shock waves in astrophysical plasma are almost always operating on scales that are much smaller than the particle collisional mean free path. Such collisionless shocks require plasma kinetic processes to decelerate the dominant incident bulk flow and “dissipate” that incident energy flux. These processes operate differently on the different plasma species and electromagnetic fields, and over different scales. They are responsible for preferential heating together with the acceleration to high energies of sub-populations of par-

49 ticles (Kucharek et al., 2003). The bow shock formed by the interaction of the super-
50 sonic solar wind flow with the Earth’s magnetosphere has long been a prime laboratory
51 for investigating collisionless shock physics thanks to its accessibility by ever-increasing
52 high quality in situ satellite observations (Burgess & Scholer, 2015; Schwartz, 2006; Schwartz
53 et al., 2013; Krasnoselskikh et al., 2013; Tsurutani & Stone, 1985; Stone & Tsurutani,
54 1985; Scudder et al., 1986).

55 The orientation of the upstream (unshocked) magnetic field plays a critical role in
56 the physics of collisionless shocks. At quasi-parallel shocks, in which the angle θ_{Bn} be-
57 tween that field and the vector normal to the shock is less than 45° , the particle gyra-
58 tion around the magnetic field is unable to confine particles on the scale of their Larmor
59 radii due to their mobility parallel to the field. The result is an extended “foreshock”
60 region (Eastwood et al., 2005) where backstreaming particles drive instabilities that re-
61 sult in large-amplitude magnetic disturbances and attendant accelerated particles.

62 The region downstream of the quasi-parallel shock (Burgess et al., 2005) is also much
63 more turbulent than that behind a quasi-perpendicular shock. This quasi-parallel mag-
64 netosheath is of interest for several reasons. Firstly, recent work by Matthaeus et al. (2020)
65 has considered it from the perspective of fundamental turbulence, comparing the tur-
66 bulence spectrum and properties to the fully developed turbulence found in solar wind.
67 The sheath turbulence is somewhat intermittent, implying that there are coherent struc-
68 tures embedded within it. They re-cast the energy equations, isolating terms via their
69 so-called “ $\Pi-D$ ” formulation to distinguish reversible energy exchange, such as adia-
70 batic compression, from irreversible dissipation. They do not find any strong correlation
71 between that dissipation and, e.g., regions of intense currents.

72 Retinò et al. (2007) reported early evidence of localized current sheets that were
73 in the process of magnetically reconnecting. In the context of turbulence in collisionless
74 plasmas, reconnection is thought to be a possible mechanism for the dissipation of en-
75 ergy that has cascaded from larger scales down to kinetic scales. Magnetic reconnection
76 also relaxes the field topology as it heats or accelerates the particles. More recently, us-
77 ing high-resolution data from the Magnetospheric Multiscale (MMS) mission, Phan et
78 al. (2018) found examples in the magnetosheath of reconnecting current sheets at small,
79 electron scales in which only the electrons participate in the reconnection process. This
80 work highlights the electron-only microphysics within complex turbulent environments.

81 By contrast, reconnection on larger scales associated with macroscopic boundaries and
82 topological changes, such as that at the magnetopause, results in ion acceleration and
83 jets at scales larger than the electron diffusion region. Ongoing work, (e.g, Wilder et al.,
84 2018; Stawarz et al., 2019), has pursued the reconnection process, associated turbulence
85 and statistics within the magnetosheath.

86 Gingell et al. (2019) found small-scale reconnection events within the transition layer
87 at a quasi-parallel shock in both MMS data and simulation results. Wang et al. (2019)
88 and Bessho et al. (2020) have extended these results to other shock geometries. These
89 current sheets appear to be localized at/near the shock itself (Gingell et al., 2020) and
90 are believed to represent a collisionless mechanism that contributes to the overall shock
91 dissipation and field topology relaxation, driving the system toward a more homogeneous
92 equilibrium plasma state.

93 To date, there has not been a comprehensive study of the specific role of thin cur-
94 rent structures in energy re-distribution throughout the magnetosheath. This is clearly
95 related to the turbulence laboratory that this region of geospace offers. However, here
96 we focus on the fact that the magnetosheath represents the downstream state of the bow
97 shock, and a state that is still far from the uniform thermal equilibrium of textbook shocks
98 in collisional fluids. We shall address the question: What role do small intense current
99 structures downstream of the quasi-parallel shock play in the overall shock energetics?
100 We address this question through a relatively unique volume of burst mode data taken
101 during a single traversal of the sub-solar magnetosheath by the MMS spacecraft.

102 The next section summarizes both the data and our primary analysis methods. We
103 then present our Results and provide some Discussion before drawing our final Conclu-
104 sions.

105 **2 Data and Methodology**

106 Our primary results are drawn from the Magnetospheric Multiscale mission (MMS)
107 (Burch, Moore, et al., 2016). We also used data from both the Wind and Artemis space-
108 craft to establish the prevailing interplanetary conditions. An overview of the traversal
109 of the terrestrial magnetosheath is shown in Figure 1, with the burst-mode data expanded
110 in Figure 2. The analysis relies on data from the Fast Plasma Investigation (FPI) (Pollock
111 et al., 2016), Fluxgate Magnetometer (FGM) (Russell et al., 2016) and electric field in-

112 strumentation (Torbert et al., 2016; Ergun et al., 2016; Lindqvist et al., 2016). We will
 113 concentrate on the latter half of this outbound traversal which corresponds to conditions
 114 behind the quasi-parallel shock under steady interplanetary conditions (see Figure 1g
 115 and Figure S1 in the Supporting Information). The MMS trajectory was nearly radial
 116 and encountered the bow shock close to the sub-solar point (Figure 1h). Figure 1 shows
 117 that the quasi-parallel magnetosheath is highly turbulent, and that there is ongoing de-
 118 celeration, compression and heating with distance behind the bow shock. Fortuitously,
 119 MMS burst mode data are available almost continuously (see Figure 2) throughout this
 120 encounter with the turbulent quasi-parallel sheath region.

121 [Figure 1 about here.]

122 The solar wind parameters deduced from Wind (see Figure S1 of the Supporting
 123 Information) are: number density $n = 3.34\text{cm}^{-3}$, proton and electron temperatures $T_p =$
 124 4.55eV , $T_e = 13.9\text{eV}$, speed $V_{sw} = 400\text{km/s}$, and average GSE magnetic field vector
 125 $\mathbf{B} = (4.08, 1, 51, 0.079)\text{nT}$ with $|\mathbf{B}| = 4.35\text{nT}$. The normal to the bow shock, found
 126 by scaling a model bow shock (Slavin & Holzer, 1981; Schwartz, 1998) to the MMS cross-
 127 ing, was $(0.993, 0.036, 0.111)\text{GSE}$, reflecting the location very near to the sub-solar point.
 128 These values lead to a plasma $\beta = 1.3$, an Alfvén mach number of 7.7 and a fast mag-
 129 netosonic mach number of 6.5. The shock geometry was $\theta_{Bn} \sim 19^\circ$.

130 We use the curlometer four-spacecraft method (Chanteur, 1998; Dunlop & East-
 131 wood, 2008) to determine the electric current density \mathbf{j} . We take advantage of the 30 ms
 132 FPI electron measurements to compute the electric field $\mathbf{E}' = \mathbf{E} + \mathbf{v}_e \times \mathbf{B}$ in the elec-
 133 tron rest frame smoothed to match the 30 ms electron cadence, where \mathbf{v}_e is the bulk elec-
 134 tron fluid velocity and \mathbf{B} is the magnetic field. We calculate \mathbf{E}' at the barycenter of the
 135 tetrahedron by combining data from the four spacecraft, to match the curlometer esti-
 136 mation of \mathbf{j} . We then calculate the energy conversion (Swisdak et al., 2018) between fields
 137 and particles, namely $\mathbf{j} \cdot \mathbf{E}'$. Positive values of $\mathbf{j} \cdot \mathbf{E}'$ correspond to energy conversion
 138 from the fields to the particles. Note that, apart from the lower cadence of the data, em-
 139 ploying the ion velocity instead of \mathbf{v}_e will lead to the same energy transfer rate, as the
 140 difference between the two expressions is $\mathbf{j} \cdot (\mathbf{v}_i - \mathbf{v}_e) \times \mathbf{B} \propto \mathbf{j} \cdot \mathbf{j} \times \mathbf{B} = \mathbf{0}$ in a singly ion-
 141 ized plasma (Zenitani et al., 2011). Other MMS data shown are drawn from MMS1.

142 [Figure 2 about here.]

143 Our event selection identifies instances of high current densities, specifically ones
 144 in which the magnitudes are 3σ above the average for the entire interval. We then se-
 145 lect manually the region surrounding that peak in \mathbf{j} that captures the full current struc-
 146 ture. One such example is shown in Figure 3. The Supporting Information includes sim-
 147 ilar plots for all 59 events. This event displays a near magnetic null coincident with a
 148 reversal in the B_y component, reminiscent of reconnecting current sheets (Burch, Tor-
 149 bert, et al., 2016). There is a rise in the particle pressures (panel g) due primarily to a
 150 rise in density (not shown), as the ion temperature decreases there. Total pressure bal-
 151 ance is maintained across the event. There is a clear signature in $\mathbf{j} \cdot \mathbf{E}'$ (panel e) which
 152 is much reduced outside the event even where there are significant current and field val-
 153 ues. We are primarily interested in the contribution of these events to the energy bud-
 154 get mediated by the bow shock and its evolution within the magnetosheath. Toward that
 155 end, we have integrated $\mathbf{j} \cdot \mathbf{E}'$ across the event, shown in the text label in Figure 3e.

156 [Figure 3 about here.]

157 As can be seen in Figure 2e, the 3σ events are distributed roughly uniformly through-
 158 out the turbulent sheath interval, so either an individual event survives this entire traver-
 159 sal or, more likely, it lasts some time and is replaced by an equivalent structure. Since
 160 the spacecraft is moving slowly with respect to the sheath flow, a time average is equiv-
 161 alent to a spatial average within the turbulent sheath. Thus the average energy conver-
 162 sion rate per unit volume in the magnetosheath is simply the sum of $\mathbf{j} \cdot \mathbf{E}'$ integrated
 163 across all the observed events divided by the total observation time T_{obs} , i.e.,

$$\mathcal{E} = \frac{1}{T_{obs}} \sum \int \mathbf{j} \cdot \mathbf{E}' dt \quad (1)$$

164 We assume for simplicity that the events are all locally planar current sheets and ori-
 165 ented perpendicular to a constant sheath flow. Then the volume of the sheath is pro-
 166 portional to the distance L throughout which the exchange (1) is occurring, so the en-
 167 ergy conversion rate per unit area, compared to the incident ram energy flux at the bow
 168 shock, is:

$$\frac{\mathcal{F}_L}{\mathcal{F}_{SW}} = \frac{(L/T_{obs}) \sum \int \mathbf{j} \cdot \mathbf{E}' dt}{V_{sw} \rho V_{sw}^2 / 2} \quad (2)$$

3 Results

We looked at 59 current structures that matched our 3σ of $\langle |\mathbf{j}| \rangle$ selection criterion. These included 27 events with magnetic depressions/near nulls, as that in Figure 3 and possible electron velocity jets parallel to the reversing field as found in magnetic reconnection sites, 14 which appeared to be tangential discontinuities lacking a dip in $|\mathbf{B}|$ and with constant total pressure, 3 which resembled rotational discontinuities with constant magnetic field strength, 6 which were reminiscent of flux ropes with a peak in $|\mathbf{B}|$ and total pressure, 3 which resembled steepened ULF waves with trailing wavetrains and 6 others. This classification is based on a qualitative assessment of variations of the parameters by inspection of plots identical in format to Figure 3, and is shown in Table S1 of the Supporting Information for all events together with the individual energy conversion values. We have not attempted a detailed analysis of, e.g., the traditional lmn geometry for each event; we provide the event details in the Supporting Information for use in future studies.

The 59 events have an average duration of 2.8s. Taken together, they make up only 3% of the roughly 90 minute quasi-parallel magnetosheath traversal in which they were observed. Based on our assumption that the events are planar, they thus fill $\sim 3\%$ of the volume of the magnetosheath. Can such a small volume process a significant amount of energy?

Figure 4 summarizes the energy conversion statistics for all the events. Most of the events (nearly 75%) have positive integrated $\mathbf{j}\cdot\mathbf{E}'$ indicating that they convert field energy into particle energy on the average. Summing over all 59 events, Equation (2) reveals that the net conversion of $4.0\times 10^{-9}\text{Ws/m}^3$ corresponds to $\sim 5\%$ of the incident solar wind ram energy flux. By way of comparison, the rise in electron enthalpy flux across the bow shock itself is $\sim 20\%$ of the ram energy flux, while the increase in electron enthalpy flux from just downstream of the bow shock (at 07:50 where $T_e \sim 40\text{ eV}$) to the downstream edge of the quasi-parallel magnetosheath (at 06:45 where $T_e \sim 55\text{ eV}$) represents $\sim 7.5\%$ of that same incident ram energy flux. These comparisons reveal that the isolated current events studied here are energetically comparable to both the heating at the bow shock itself and to the continued increase in electron temperature with downstream distance. We discuss below the caution that should be applied here, since

200 $\mathbf{j}\cdot\mathbf{E}'$ is the total energy conversion, including bulk flow, adiabatic compression and ir-
 201 reversible dissipation.

202 As a final note here, we have seen that these current events can have both posi-
 203 tive and negative energy conversions. In terms of their overall impact on the energet-
 204 ics of the sheath, we have calculated the total energy processed by the events regardless
 205 of sign by summing $|\mathbf{j}\cdot\mathbf{E}'|$. This conversion is $8.9\times 10^{-9}\text{Ws/m}^3$, corresponding to 11%
 206 of the incident ram energy flux.

207 [Figure 4 about here.]

208 4 Discussion

209 Our results show that isolated current structures within the magnetosheath down-
 210 stream of the quasi-parallel bow shock convert electromagnetic field energy into parti-
 211 cle energy at a rate that is comparable to the increase in electron enthalpy flux within
 212 the magnetosheath, and 25% of the change in that enthalpy flux occurring at the shock
 213 itself. If that conversion is all irreversible, this implies that roughly 20% of the electron
 214 heating from the solar wind to deep in the magnetosheath is (a) distributed throughout
 215 the magnetosheath and (b) localized in space to the most intense currents. However, the
 216 electro-fluid dynamics can't distinguish irreversible heating from reversible compression
 217 or accelerated flows. Recent work in the context of plasma turbulence (Matthaeus et al.,
 218 2020) has attempted to separate out these different energy reservoirs. They conclude that
 219 there is no direct correlation between the intense current sheets and their $\Pi-D$ mea-
 220 sure of dissipation (Bandyopadhyay et al., 2020), although they do find that dissipation
 221 is highly spatially localized near to intense current events. We note in this context that
 222 most of our events, such as that shown in Figure 3, do not show significant temperature
 223 changes within them.

224 However, our goal here is simpler, namely to establish whether intense currents are
 225 significant in terms of the overall shock and sheath energetics. For the case studied here
 226 the total energy conversion (ignoring the sign) is approximately 11% of the ram energy
 227 flux incident at the bow shock. This is indicative of the incompleteness of the bow shock
 228 in thermalizing the incident ram energy and of the ongoing dissipation, redistribution,
 229 and relaxation of the plasma through the entire magnetosheath. Yet this specific energy
 230 conversion is mediated by only $\sim 3\%$ of the volume of the magnetosheath.

5 Conclusions

We have studied the exchange between particle and electromagnetic energy downstream of the quasi-parallel Earth's bow shock through the analysis of a traversal of the sub-solar magnetosheath by MMS. The interplanetary conditions were steady, and an unusually long interval of burst mode data was available. Our main conclusion is that thin current events or sheets, which are approximately 3 s in duration and thus occupy 3% of the magnetosheath volume, process nearly 11% of the bulk flow ram energy incident at the bow shock. In this example, that energy conversion was predominantly from field energy to particle energy. We are not able to determine whether that represents irreversible dissipation or reversible compressions (Matthaeus et al., 2020), nor the partition of that particle energy between electrons and ions. Nonetheless, our results show the importance of these isolated thin current structures in the energy processing that is initiated at the bow shock but continues far into the downstream region.

The region downstream of a quasi-parallel shock is well-known to be turbulent (Lucek et al., 2005; Burgess et al., 2005) which promotes the formation of thin current structures. The fluctuation levels, and hence current sheet intensities, downstream of the quasi-perpendicular bow shock are much less. This can even be seen in the first third of Figure 1(a-f) before the interplanetary field turned to more quasi-parallel geometries. These regions show less evolution in density compression or temperature, suggesting that the binding of the particles and fields by the perpendicular geometry promotes more rapid energy exchange. There may nonetheless be subtle changes within individual particle populations as, e.g., anisotropy-driven instabilities relax these populations toward thermal equilibrium. This could be productively explored in a similar future study of this kind. Upstream disturbances such as hot flow anomalies and foreshock bubbles, together with higher levels of interplanetary turbulence, may also lead to higher levels of magnetosheath turbulence which again could promote more numerous and intense current sheets even under quasi-perpendicular geometries.

Acknowledgments

Artemis and Wind data were drawn from the SPDF/CDAWEB repository (<https://cdaweb.gsfc.nasa.gov/index.html/>). We gratefully acknowledge the respective instrument teams and archive curators. MMS data can be found at the MMS public Science Data Center (<https://lasp.colorado.edu/mms/sdc/public/>). All the data anal-

263 ysis and graphics were performed using the opensource QSAS Science Analysis System
 264 (<https://sourceforge.net/projects/qsas/>). This work was supported by NASA Award
 265 80NSSC19K0849 together with NASA MMS contracts to the instrument teams. IG is
 266 supported by a Royal Society URF.

267 References

- 268 Bandyopadhyay, R., Matthaeus, W. H., Parashar, T. N., Yang, Y., Chasapis, A.,
 269 Giles, B. L., ... Burch, J. L. (2020, June). Statistics of Kinetic Dissipation
 270 in the Earth's Magnetosheath: MMS Observations. *Phys. Rev. Lett.*, *124*(25),
 271 255101. doi: 10.1103/PhysRevLett.124.255101
- 272 Bessho, N., Chen, L. J., Wang, S., Hesse, M., Wilson, I., L. B., & Ng, J. (2020,
 273 September). Magnetic reconnection and kinetic waves generated in the
 274 Earth's quasi-parallel bow shock. *Phys. Plasmas*, *27*(9), 092901. doi:
 275 10.1063/5.0012443
- 276 Burch, J. L., Moore, T. E., Torbert, R. B., & Giles, B. L. (2016, March). Magne-
 277 tospheric Multiscale Overview and Science Objectives. *Space Sci. Rev.*, *199*, 5-
 278 21. doi: 10.1007/s11214-015-0164-9
- 279 Burch, J. L., Torbert, R. B., Phan, T. D., Chen, L. J., Moore, T. E., Ergun, R. E.,
 280 ... Chandler, M. (2016, June). Electron-scale measurements of magnetic
 281 reconnection in space. *Science*, *352*, aaf2939. doi: 10.1126/science.aaf2939
- 282 Burgess, D., Lucek, E. A., Scholer, M., Bale, S. D., Balikhin, M. A., Balogh, A., ...
 283 Walker, S. N. (2005, June). Quasi-parallel Shock Structure and Processes. *Sp.*
 284 *Sci. Rev.*, *118*(1-4), 205-222. doi: 10.1007/s11214-005-3832-3
- 285 Burgess, D., & Scholer, M. (2015). *Collisionless Shocks in Space Plasmas*. Cam-
 286 bridge University Press.
- 287 Chanteur, G. (1998, January). Spatial Interpolation for Four Spacecraft: Theory.
 288 *ISSI Scientific Reports Series*, *1*, 349-370.
- 289 Dunlop, M. W., & Eastwood, J. P. (2008, January). The Curlometer and Other Gra-
 290 dient Based Methods. *ISSI Scientific Reports Series*, *8*, 17-26.
- 291 Eastwood, J. P., Lucek, E. A., Mazelle, C., Meziane, K., Narita, Y., Pickett, J., &
 292 Treumann, R. A. (2005, June). The Foreshock. *Sp. Sci. Rev.*, *118*(1-4), 41-94.
 293 doi: 10.1007/s11214-005-3824-3
- 294 Ergun, R. E., Tucker, S., Westfall, J., Goodrich, K. A., Malaspina, D. M., Summers,

- 295 D., ... Cully, C. M. (2016, March). The Axial Double Probe and Fields
 296 Signal Processing for the MMS Mission. *Space Sci. Rev.*, *199*, 167-188. doi:
 297 10.1007/s11214-014-0115-x
- 298 Gingell, I., Schwartz, S. J., Eastwood, J. P., Burch, J. L., Ergun, R. E., Fuselier, S.,
 299 ... Wilder, F. (2019, February). Observations of Magnetic Reconnection in
 300 the Transition Region of Quasi-Parallel Shocks. *Geophys. Res. Lett.*, *46*(3),
 301 1177-1184. doi: 10.1029/2018GL081804
- 302 Gingell, I., Schwartz, S. J., Eastwood, J. P., Stawarz, J. E., Burch, J. L., Ergun,
 303 R. E., ... Wilder, F. (2020, January). Statistics of Reconnecting Current
 304 Sheets in the Transition Region of Earth's Bow Shock. *J. Geophys. Res.*,
 305 *125*(1), e27119. doi: 10.1029/2019JA027119
- 306 Krasnoselskikh, V., Balikhin, M., Walker, S. N., Schwartz, S., Sundkvist, D.,
 307 Lobzin, V., ... Comisel, H. (2013, October). The Dynamic Quasiperpen-
 308 dicular Shock: Cluster Discoveries. *Sp. Sci. Rev.*, *178*(2-4), 535-598. doi:
 309 10.1007/s11214-013-9972-y
- 310 Kucharek, H., Möbius, E., Li, W., Farrugia, C. J., Popecki, M. A., Galvin, A. B.,
 311 ... Bochsler, P. A. (2003, October). On the source and acceleration of en-
 312 ergetic He⁺: A long-term observation with ACE/SEPICA. *J. Geophys. Res.*,
 313 *108*(A10), 8040. doi: 10.1029/2003JA009938
- 314 Lindqvist, P.-A., Olsson, G., Torbert, R. B., King, B., Granoff, M., Rau, D.,
 315 ... Tucker, S. (2016, March). The Spin-Plane Double Probe Elec-
 316 tric Field Instrument for MMS. *Space Sci. Rev.*, *199*, 137-165. doi:
 317 10.1007/s11214-014-0116-9
- 318 Lucek, E. A., Constantinescu, D., Goldstein, M. L., Pickett, J., Pinçon, J. L.,
 319 Sahraoui, F., ... Walker, S. N. (2005, June). The Magnetosheath. *Sp. Sci.*
 320 *Rev.*, *118*(1-4), 95-152. doi: 10.1007/s11214-005-3825-2
- 321 Matthaeus, W. H., Yang, Y., Wan, M., Parashar, T. N., Bandyopadhyay, R.,
 322 Chasapis, A. r., ... Valentini, F. (2020, March). Pathways to Dissi-
 323 pation in Weakly Collisional Plasmas. *Astrophys. J.*, *891*(1), 101. doi:
 324 10.3847/1538-4357/ab6d6a
- 325 Phan, T. D., Eastwood, J. P., Shay, M. A., Drake, J. F., Sonnerup, B. U. Ö., Fu-
 326 jimoto, M., ... Magnes, W. (2018, May). Electron magnetic reconnection
 327 without ion coupling in Earth's turbulent magnetosheath. *Nature*, *557*(7704),

- 328 202-206. doi: 10.1038/s41586-018-0091-5
- 329 Pollock, C., Moore, T., Jacques, A., Burch, J., Gliese, U., Saito, Y., ... others
 330 (2016, March). Fast Plasma Investigation for Magnetospheric Multiscale. *Space*
 331 *Sci. Rev.*, *199*, 331-406. doi: 10.1007/s11214-016-0245-4
- 332 Retinò, A., Sundkvist, D., Vaivads, A., Mozer, F., André, M., & Owen, C. J. (2007,
 333 April). In situ evidence of magnetic reconnection in turbulent plasma. *Nat.*
 334 *Phys.*, *3*(4), 236-238. doi: 10.1038/nphys574
- 335 Russell, C. T., Anderson, B. J., Baumjohann, W., Bromund, K. R., Dearborn,
 336 D., Fischer, D., ... Richter, I. (2016, March). The Magnetospheric Mul-
 337 tiscale Magnetometers. *Space Sci. Rev.*, *199*, 189-256. doi: 10.1007/
 338 s11214-014-0057-3
- 339 Schwartz, S. J. (1998, January). Shock and Discontinuity Normals, Mach Numbers,
 340 and Related Parameters. *ISSI Scientific Reports Series*, *1*, 249-270.
- 341 Schwartz, S. J. (2006, June). Shocks: Commonalities in Solar-Terrestrial Chains. *Sp.*
 342 *Sci. Rev.*, *124*(1-4), 333-344. doi: 10.1007/s11214-006-9093-y
- 343 Schwartz, S. J., Zweibel, E. G., & Goldman, M. (2013, October). Microphysics in
 344 Astrophysical Plasmas. *Sp. Sci. Rev.*, *178*(2-4), 81-99. doi: 10.1007/s11214-013
 345 -9975-8
- 346 Scudder, J. D., Mangeney, A., Lacombe, C., Harvey, C. C., Wu, C. S., & Anderson,
 347 R. R. (1986, October). The resolved layer of a collisionless, high β , supercrit-
 348 ical, quasi-perpendicular shock wave, 3. Vlasov electrodynamics. *J. Geophys.*
 349 *Res.*, *91*(A10), 11075-11098. doi: 10.1029/JA091iA10p11075
- 350 Slavin, J. A., & Holzer, R. E. (1981, December). Solar wind flow about the ter-
 351 restrial planets, 1. Modeling bow shock position and shape. *J. Geophys. Res.*,
 352 *86*(A13), 11401-11418. doi: 10.1029/JA086iA13p11401
- 353 Stawarz, J. E., Eastwood, J. P., Phan, T. D., Gingell, I. L., Shay, M. A., Burch,
 354 J. L., ... Franci, L. (2019, June). Properties of the Turbulence Associated
 355 with Electron-only Magnetic Reconnection in Earth's Magnetosheath. *Astro-*
 356 *phys. J. Lett.*, *877*(2), L37. doi: 10.3847/2041-8213/ab21c8
- 357 Stone, R. G., & Tsurutani, B. T. (1985, January). Collisionless shocks in the helio-
 358 sphere. A tutorial review. *Washington DC American Geophysical Union Geo-*
 359 *physical Monograph Series*, *34*. doi: 10.1029/GM034
- 360 Swisdak, M., Drake, J. F., Price, L., Burch, J. L., Cassak, P. A., & Phan, T. D.

- 361 (2018, June). Localized and Intense Energy Conversion in the Diffusion Re-
 362 gion of Asymmetric Magnetic Reconnection. *Geophys. Res. Lett.*, *45*(11),
 363 5260-5267. doi: 10.1029/2017GL076862
- 364 Torbert, R. B., Russell, C. T., Magnes, W., Ergun, R. E., Lindqvist, P.-A., LeCon-
 365 tel, O., ... Lappalainen, K. (2016, March). The FIELDS Instrument Suite
 366 on MMS: Scientific Objectives, Measurements, and Data Products. *Space Sci.*
 367 *Rev.*, *199*, 105-135. doi: 10.1007/s11214-014-0109-8
- 368 Tsurutani, B. T., & Stone, R. G. (1985, January). Collisionless shocks in the he-
 369 liosphere: Reviews of current research. *Washington DC American Geophysical*
 370 *Union Geophysical Monograph Series*, *35*. doi: 10.1029/GM035
- 371 Wang, S., Chen, L.-J., Bessho, N., Hesse, M., Wilson, L. B., Giles, B., ... Burch,
 372 J. L. (2019, January). Observational Evidence of Magnetic Reconnection
 373 in the Terrestrial Bow Shock Transition Region. *Geophys. Res. Lett.*, *46*(2),
 374 562-570. doi: 10.1029/2018GL080944
- 375 Wilder, F. D., Ergun, R. E., Burch, J. L., Ahmadi, N., Eriksson, S., Phan, T. D., ...
 376 Khotyaintsev, Y. V. (2018, August). The Role of the Parallel Electric Field in
 377 Electron-Scale Dissipation at Reconnecting Currents in the Magnetosheath. *J.*
 378 *Geophys. Res.*, *123*(8), 6533-6547. doi: 10.1029/2018JA025529
- 379 Zenitani, S., Hesse, M., Klimas, A., & Kuznetsova, M. (2011, May). New Measure
 380 of the Dissipation Region in Collisionless Magnetic Reconnection. *Phys. Rev.*
 381 *Lett.*, *106*(19), 195003. doi: 10.1103/PhysRevLett.106.195003

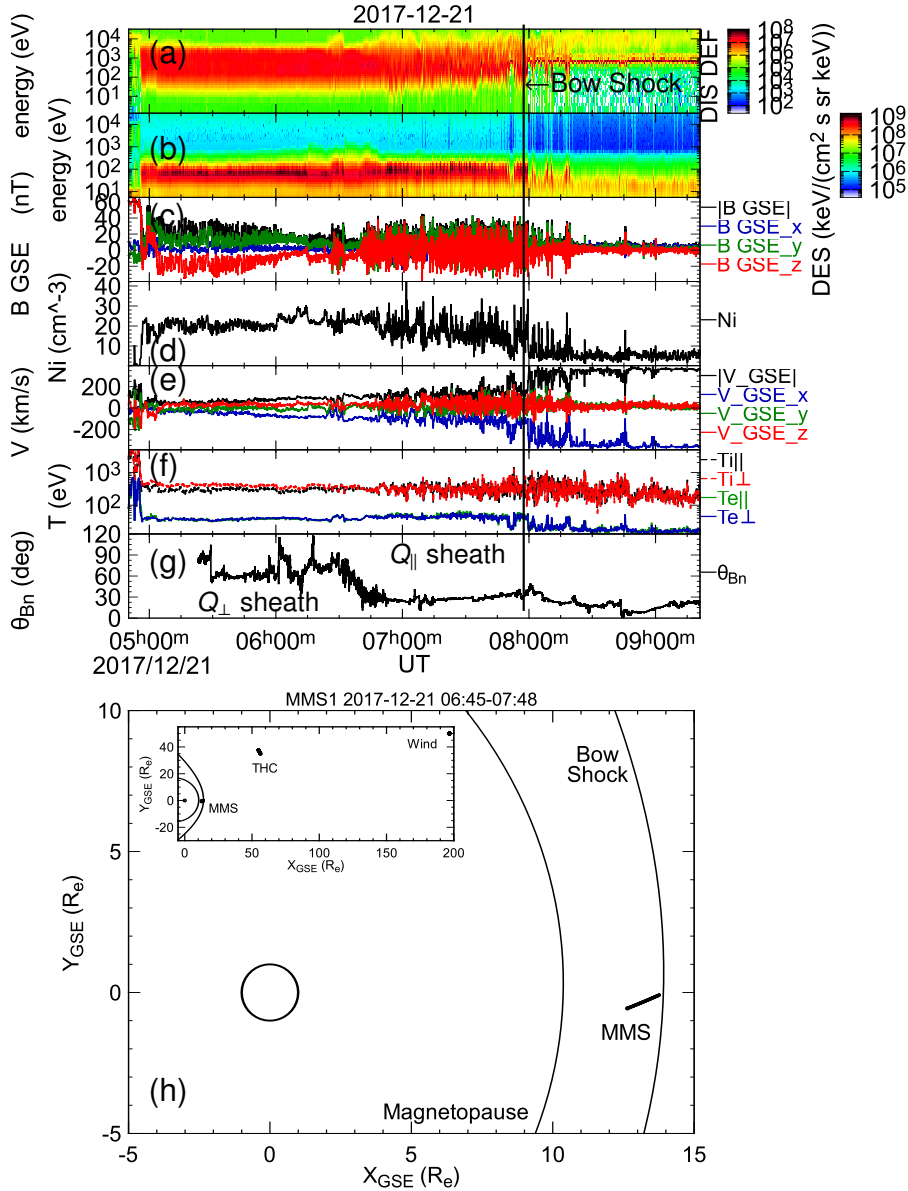


Figure 1. Top: Overview of the magnetosheath crossing by MMS1 on 2017/12/21. Ion (a) and electron (b) differential energy fluxes, (c) magnetic field in GSE, (d) ion density (e) ion flow velocity (f) electron and ion temperatures parallel and perpendicular to the local magnetic field and (g) angle between the interplanetary magnetic field (lagged in time from the WIND spacecraft) and the normal to a model of the Earth’s bow shock. Bottom: (h) Trajectory of MMS showing an essentially sub-solar traversal of the magnetosheath together with (inset) the locations of THC (Artemis) and Wind spacecraft which were used to determine the lagged inter-planetary plasma conditions. The four MMS spacecraft were separated by ~ 25 km.

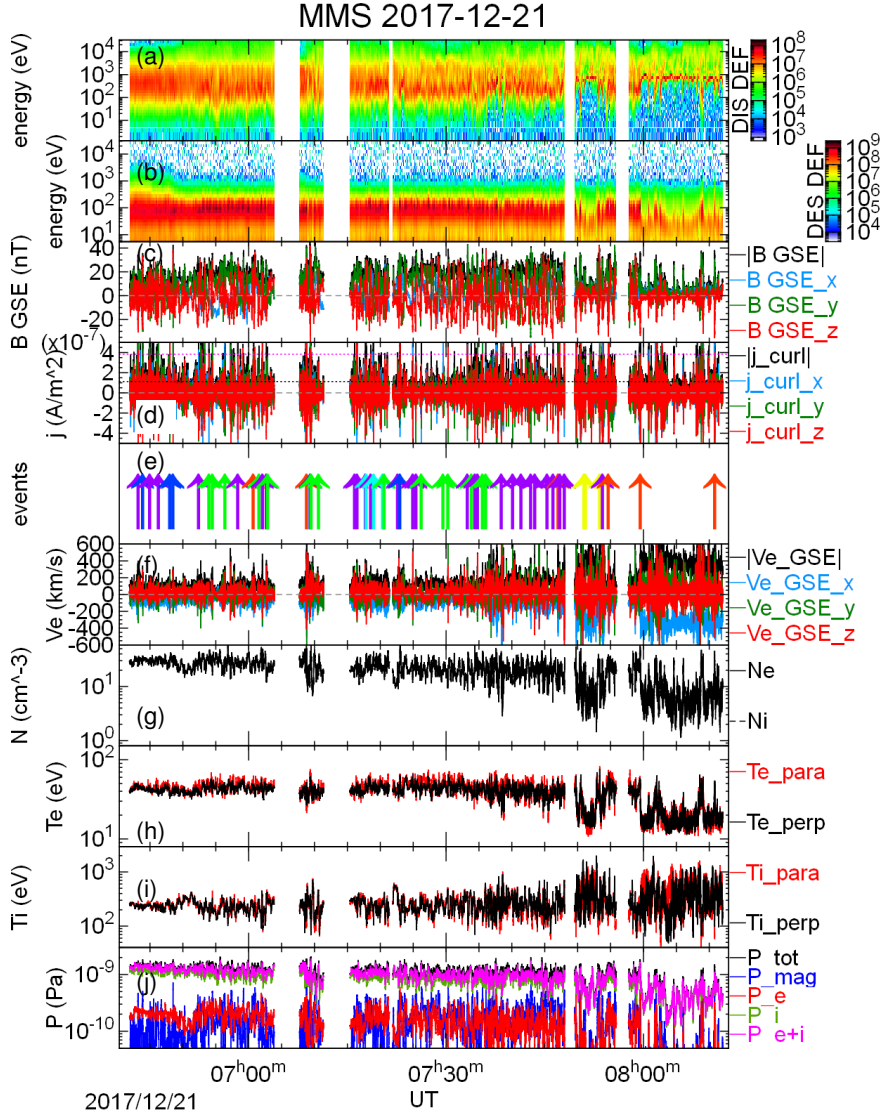


Figure 2. Overview of the burst-mode data from the MMS quasi-parallel sheath crossing observed on 2017-12-21. All data are from MMS1 except the current density. Ion (a) and electron (b) differential energy fluxes in $\text{keV}/(\text{cm}^2 \text{ s sr keV})$ (c) magnetic field in GSE, (d) electric current density calculated from a curlometer technique. Dotted lines show the 1σ and 3σ $|j|$ levels (e) selected events with $|j| > 3\sigma$, color coded by probable type of current structure (see text and Figure 4 below) (f) electron bulk flow velocity (g) electron and ion plasma densities (indistinguishable on this scale) (h) electron and (i) ion temperatures parallel and perpendicular to the local magnetic field and (j) plasma, field and total pressure.

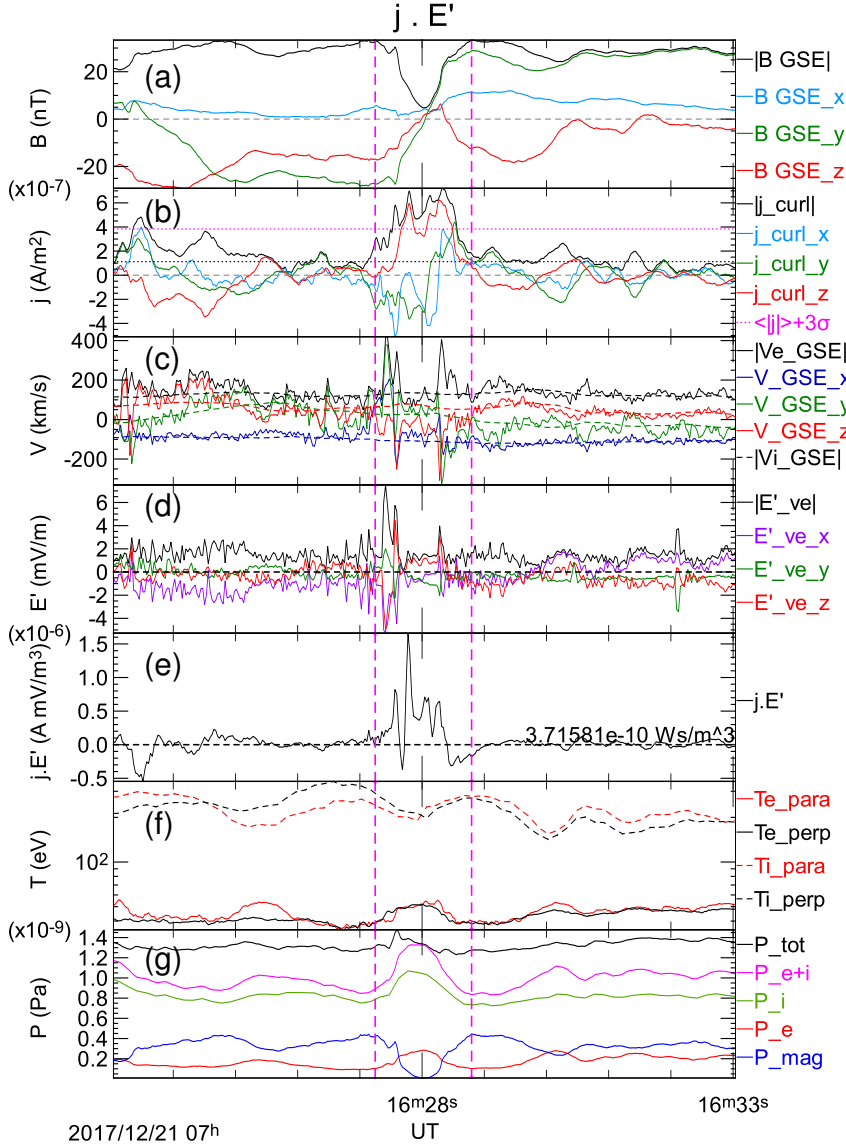


Figure 3. An example of the current sheets/structures selected for this study. Data from MMS1 except in (b) and (e) Top to bottom (a) magnetic field in GSE (b) current density \mathbf{j} in GSE calculated via the curlometer method (c) electron (solid) and ion (dashed) bulk flow velocities (d) DC electric field transformed into the electron flow frame (e) energy conversion rate $\mathbf{j} \cdot \mathbf{E}'$ based on \mathbf{E}' calculated at the barycenter of the four spacecraft tetrahedron (f) electron (solid) and ion (dashed) temperatures parallel (red) and perpendicular (black) to the instantaneous magnetic field (g) magnetic, particle, and total plasma pressure. Note the current density rises above the dashed 3σ line in panel (b), and the region surrounding this selected manually as the full event delineated by dashed vertical magenta lines. The integral of $\mathbf{j} \cdot \mathbf{E}'$ over the event is shown in panel (e).

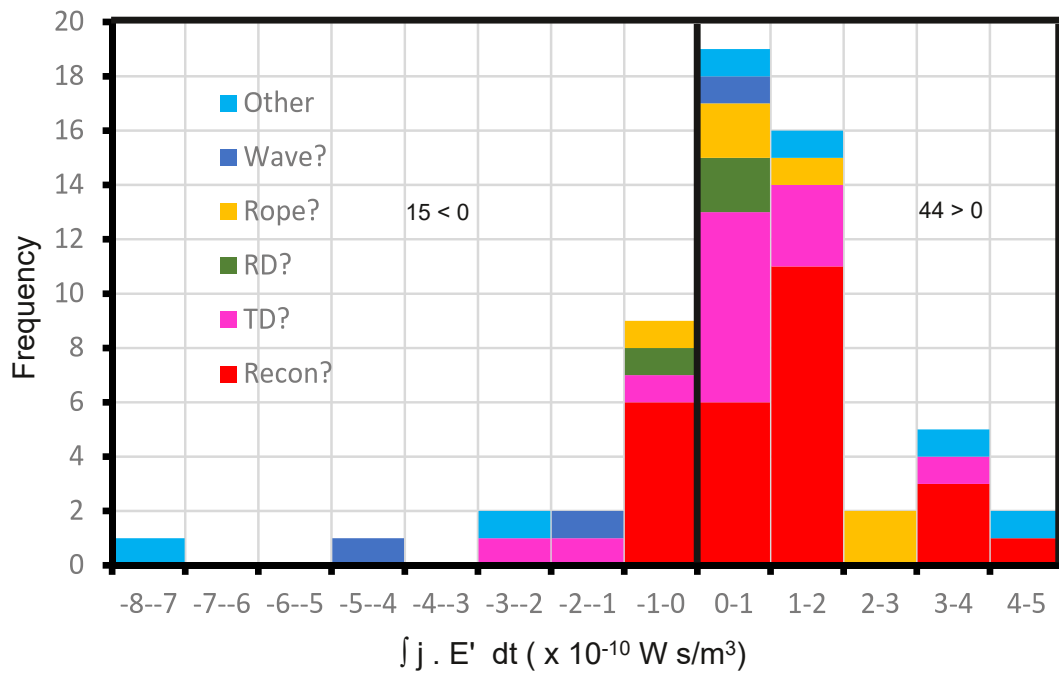


Figure 4. Statistics of the integrated energy conversion $\int \mathbf{j} \cdot \mathbf{E}' dt$ for the 59 events in this study, broken down by the apparent type of the event (see text).